

A DISCRETE MODEL FOR ALKALI-SILICA-REACTION IN CONCRETE

M. ALNAGGAR*, G. CUSATIS* AND G. DI LUZIO†

*Northwestern University,
Department of Civil and Environmental Engineering
Evanston, IL 60208, USA
e-mail: MohammedAlnaggar2012@u.northwestern.edu,
e-mail: g-cusatis@northwestern.edu, web page: <http://www.cusatis.us>

†Politecnico di Milano,
Department of Structural Engineering (DIS)
Piazza Leonardo da Vinci, 32 - 20133 Milano, Italy
e-mail: diluzio@stru.polimi.it, web page: <http://www.stru.polimi.it/people/diluzio>

Key words: Cohesive Fracture, Alkali-Silica Reaction, Lattice Discrete Particle Model, Durability

Abstract. The safety and durability of a large number of structures, especially in high humidity environments, are endangered by Alkali-Silica Reaction (ASR). ASR is characterized by two processes: the first is the formation of gel which happens when water transmitted alkali come in contact with reactive silica in aggregates; the second is the imbibition of water into this formed basic gel and the consequent swelling, which, in turn, causes deterioration of concrete internal structure by a diffuse cracking. In this paper, the ASR effect on concrete deterioration is implemented within the framework of a mesoscale formulation, the Lattice Discrete Particle Model (LDPM), that simulates the heterogeneity of the concrete internal structure as well as the thermo-chemo-mechanical characteristics of the ASR reaction. The proposed formulation allows a precise and unique modeling of ASR effect including non-uniform expansions, expansion transfer and heterogeneous cracking. The model can replicate ASR cracking behavior in free and confined expansion tests. This paper presents calibration and validation of the present model on the basis of experiments for unrestrained specimens under various axial loadings undergoing ASR expansion. The results show good agreement with the experimental data.

1 INTRODUCTION

ASR effect is reported in many concrete structures all around the world, especially those built in high humidity environments [1]. Temperature plays a fundamental role in the ASR rate of reaction [2] – the higher the temperature the faster is the reaction. However, even in countries with average low temperatures ASR is reported to be a serious problem for the durability of concrete structures. The effect of ASR is a progressive deterioration and loss of concrete stiffness and strength that results from the

long term formation and expansion of ASR gel which, in turn, induce internal pressure on the concrete meso-structure. This pressure causes non uniform deformations leading to cracking. While the chemical representation of the reaction was addressed intensively in the literature, the fracture mechanics associated with the progressive expansion is not as much addressed.

In this paper, the chemical model of ASR is based on the model proposed by Bažant and Steffens [3], extended hereinafter to include additional factors such as temperature effect, al-

kali content in the concrete mix (Alkali content effect) and gel formation effect on water imbibition rate. The proposed model, whose predecessors were presented in recent conferences [4, 5], is implemented in the Lattice discrete particle model (LDPM) framework [6, 7] to simulate the deterioration of concrete due to ASR. LDPM simulates the mechanical interaction of coarse aggregate pieces through a system of three-dimensional polyhedral particles connected through lattice struts [6]. LDPM has been calibrated and validated extensively through the comparison to experimental data and it has shown great capabilities in modeling concrete damage, cracking and fracture [7].

2 ALKALI SILICA REACTION (ASR) MODELING

According to the model proposed by Bažant and Steffens [3] – adopted and extended in this section – the overall ASR process can be approximately described by considering that (1) for the ASR reaction to occur, water needs to be present in the pores to act as transport medium for hydroxyl and alkali ions required by the ASR reaction; (2) the expansion of the gel is basically due to water imbibition; and (3) a continuous supply of water is needed for the swelling to continue over time. As in the original paper by Bažant and Steffens [3] and consistently with the LDPM formulation, in this study the aggregate particles are assumed to have spherical shape and the whole volume of each particle is assumed to be reactive with the silica assumed to be smeared uniformly over the aggregate volume. This is certainly an approximation compared to reality in which shape and size of the aggregate particles may vary widely, as well as the content of reactive silica in flaws, inclusions, and veins. Under this approximation, however, the dissolution of silica may be assumed to progress roughly in a uniform manner in the radial direction inward from the surface.

2.1 Gel Formation

A stoichiometric relationship for the ASR reaction is very difficult to ascertain due to the great variety of possible chemical equilibria for different values of pH. In this model, as also done in Bažant and Steffens [3], the monomer H_2SiO_4^- is considered to be the unique form of basic gel produced by the dissolution process. In this case it can be stated that two water molecules are necessary to dissolve one silica atom. The thermodynamics and kinetics of the ASR reaction were studied in Refs [8, 9] and it was concluded that reaction rate is faster than the actual rate of ASR production observed in concrete structures. This led researchers to the conclusion that some other mechanism must be the dominant one and it was observed that as the reaction progresses, the unreacted silica in the interior of each of aggregate particles is shielded by a spherical layer of the reaction product, the ASR gel. Through this layer further water molecules must diffuse in order to reach the reacting surface of the particle and dissolve more silica. This diffusion slows down the ASR tremendously and becomes the process governing the rate of ASR [8, 9]. Thus, the rate of ASR gel production can be best approximated by solving a diffusion problem.

A simple characterization of water diffusion across the gel layer and towards the reaction front at the surface of the unreacted spherical aggregate volume can be obtained as follows. The diffusion is assumed to be governed by a linear Fick's law. Thus, the radial flux of water, J_w , is given by

$$J_w = a_s(T) \nabla \cdot \xi_w \quad (1)$$

where ξ_w = water concentration within the layer of ASR gel as a function of radial coordinate x , and $a_s(T)$ = permeability of ASR gel to water. The permeability is assumed to be temperature dependent as

$$a_s(T) = a_{s0} \exp\left(\frac{E_{ad}}{RT_0} - \frac{E_{ad}}{RT}\right) \quad (2)$$

where E_{ad} is the ASR activation energy, R is the universal gas constant, T_0 is a reference tem-

perature at which the reference ASR gel permeability to water a_{s0} is defined, and T is the current temperature. Equation 2 takes into account the effect of temperature on the permeability of the ASR gel, as proposed for the permeability of concrete by many authors [10–13]. It should be noted here that the time scale for temperature variation in real structures is the season length while the ASR process takes place on about 10 to 50 years, a period on which, the effect of change in temperature can be neglected. Mass conservation within infinitesimal elements of the gel requires that $\dot{\xi}_w = \nabla J_w$ (dot denotes derivative with respect to time t). One has

$$\dot{\xi}_w = a_s(T) \nabla^2 \xi_w \quad (3)$$

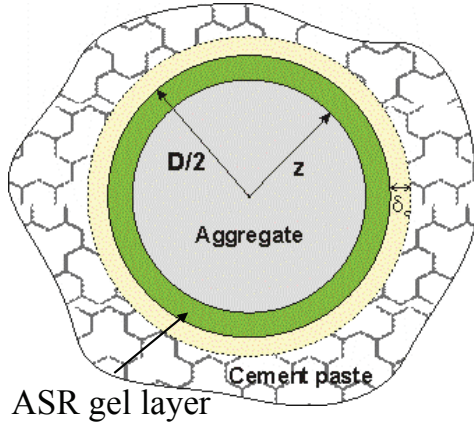


Figure 1: Idealization of gel formation in one aggregate

As discussed previously, the reaction at the silica dissolution front may be considered to be almost immediate compared to the duration of water transport to the front. Therefore, the rate of advance of the reaction front must depend solely on the rate at which the diffusion through the ASR gel layer can supply water to the reaction front. The front can advance only after enough water has been supplied to combine the silica. Consequently, for a constant temperature, the radial profile of ξ_w may be expected to be the profile of a steady-state diffusion process. This profile can be expressed as in Bažant and Steffens [3] by

$$\xi_w = w_s F(\bar{x}), F(\bar{x}) = \frac{1 - 2z/D\bar{x}}{1 - 2z/D} \quad (4)$$

where w_s = concentration of water in the concrete surrounding the particle, $F(x)$ = dimensionless concentration profile, x = radial coordinate, z = radius of the remaining unreacted particle, D = aggregate diameter, and $\bar{x} = 2x/D$ is the dimensionless radial coordinate (See Figure 1 for details).

The condition of mass balance at the reaction front $x = z$ requires that

$$r\rho_s dz = -a_s(T) \frac{\partial \xi_w}{\partial x} dt \quad (5)$$

where r = stoichiometric ratio (mass conversion ratio) = $2m_w/m_s$; $m_w = 18$ g/mole; and $m_s = 60.09$ g/mole, and this comes from the assumption that 2 water molecules are needed to dissolve one silica molecule as stated earlier in this section. Substituting $\xi_w = w_s F(\bar{x})$ according to Eq. 4 and differentiating with respect to x , one obtains the following differential equation for the velocity of the reaction front:

$$\dot{z} = \frac{2w_s D (dF(\bar{x})/d\bar{x})|_{\bar{x}=z}}{r\rho_s \tau_w} \quad (6)$$

where $\tau_w = D^2/a_s(T)$ represents the halftime of diffusion of water through the gel layer, and $a_s(T)$ is Fick's permeability (having the dimension of m^2/s). Note that the slope of the profile at the reaction front becomes vertical when $z \rightarrow 0$.

Defining the parameters $\tau_s = 4a_s(T)/D^2$, $k_s = w_s/r\rho_s$; and the nondimensional variables $\tau = tk_s/\tau_s$ and $\zeta = 2z/D$, the differential equation in Eq. 6 can be written as

$$\frac{d\zeta}{d\tau} = -[\zeta(1 - \zeta)]^{-1} \quad (7)$$

In this study, this equation was solved numerically with the given initial value $\zeta(\tau = 0) = 1$. The numerical solution was shown to exist between $\tau = 0$ and $\tau = 1/6$. At $\tau = 1/6$ the entire aggregate particle has fully reacted. For the sake of simplicity and for an efficient computational implementation, the numerical solution of Eq. 7 can be well approximated by (see

figure 2)

$$\zeta(\tau) = 1 - 2.22 \tau^{0.6} \quad \text{for } 0 \leq \tau \leq \frac{1}{12}$$

$$\zeta(\tau) = 2.22 \left(\frac{1}{6} - \tau \right)^{0.6} \quad \text{for } \frac{1}{12} < \tau \leq \frac{1}{6} \quad (8)$$

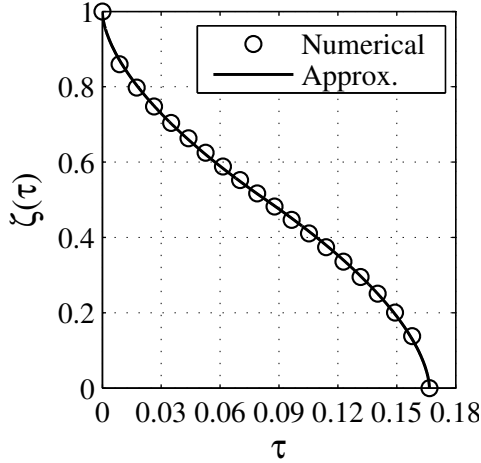


Figure 2: Numerical and approximate solutions for Eq. 7

The total mass of basic gel, ξ_g , produced in the aggregate can be then determined by

$$\xi_g = \frac{4\pi D^3}{3} (1 - \zeta^3) \frac{m_g}{m_s} \rho_s \quad (9)$$

where m_g is the molar weights of the gel (H_2SiO_4^- with $m_g = 94.1$ [g/mole]). Furthermore, the alkali content is not always present in enough quantity for the ASR reaction to occur. So, in order to account for the presence of alkali, the function $\rho_k = \min(\langle AC - AC_{th} \rangle / (AC_{req} - AC_{th}), 1)$ is introduced such that the alkali content AC is related to the required alkali content, AC_{req} to have the full reaction of silica, and to an alkali content threshold, AC_{th} at which, there is almost no expansion. Eq. 9 becomes

$$\xi_g = \frac{4\pi D^3}{3} (1 - \zeta^3) \frac{m_g}{m_s} \rho_s \rho_k \quad (10)$$

2.2 Water imbibed by ASR gel

The ASR product is a solid (gel) [14], which has the capacity – typical of colloidal systems

– to imbibe water molecules, causing extensive swelling. Since the ASR gel is constrained in the pores of concrete, the swelling must produce pressure in the gel and the surrounding concrete structure. This pressure induces the known cracking and damage to the concrete. Expansion of the ASR gel can be partly accommodated without significant pressure build up by filling the capillary pores in the hardened cement paste located close to the surface of the reactive aggregate particles. This is also facilitated by the existence of the so-called interfacial transition zone (ITZ) that is a layer of material with a higher porosity in the hardened cement paste near the aggregate surface. Similarly to the ITZ size, the thickness, δ_c , of the layer in which the capillary pores are accessible to the swelling ASR gel may be considered constant, independent of particle size D .

As already mentioned, the physical properties of the basic form of ASR gel are not yet known. But it seems logical to assume that the formation of this basic gel causes no significant volume increase per se and that all volume changes are caused solely by the intake of additional water. Denoting by w_i the mass of water imbibed by the basic gel, the volume increase of the gel is

$$\Delta V = \frac{w_i}{\rho_w} \quad (11)$$

The imbibition of water from the bulk of mortar or concrete into the basic gel cannot happen instantly. It is a local micro-diffusion process that occurs with some delay. Because the gel is expelled into the pores, the geometry of this diffusion is no longer spherical and it appears difficult to choose any particular idealized geometry of the diffusion flow of water that should be analyzed. It seems therefore appropriate to conduct merely a simplified overall analysis without reference to any particular geometry. It is reasonable to assume that

$$\dot{w}_i = \frac{A_i}{\tau_i} \quad (12)$$

where A_i characterizes the thermodynamic affinity and τ_i is a certain characteristic time.

To set up a reasonable expression for A_i , some aspects should be considered: (1) The chemical potential governing water transport through concrete may be assumed to be roughly proportional to the specific water content w_i ; (2) The water imbibition rate \dot{w}_i , and thus A_i , should be proportional to the mass of basic gel, ξ_g ; (3) The water imbibition rate \dot{w}_i should decrease with a decreasing relative humidity h in the pores of concrete near the reacting particle and should stop at relative humidity below which water is not available for ASR reaction and imbibition; (4) The water imbibition rate \dot{w}_i should decrease with a decreasing absolute temperature T of concrete and vice-versa. Such dependence can be well modeled with an Arrhenius-type equation. According to these observations and considering only the case of full saturation (typical, for example, for dams), the affinity (thermodynamic driving force or chemical potential difference) governing the water imbibition may be approximately expressed as

$$A_i = w_i^*(T, h, \xi_g) - w_i \quad (13)$$

where $w_i^*(T, h, \xi_g)$ is the value w_i at thermodynamic equilibrium, at which no water migrates into or out of the ASR gel and can be expressed as

$$w_i^*(T, h, \xi_g) = \kappa_i^0 \exp\left(\frac{E_{aw}}{RT_0} - \frac{E_{aw}}{RT}\right) \xi_g \quad (14)$$

where E_{aw} is the activation energy of the imbibition process and κ_i^0 represents the amount of water imbibed by unit mass of basic gel. Analysis of experimental data carried out in this study suggests that, in absence of more precise information about the water imbibition process, $\kappa_i^0 \approx 1$ is a reasonable assumption.

For reasons of dimensionality, the characteristic time, called the imbibition halftime, must have the form $\tau_i = \delta^2 / C_{wi} \eta(w_i)$, in which C_{wi} is the diffusivity for microdiffusion of water close to the aggregate (surely much lower than the diffusivity for global water diffusion through a concrete structure), δ is the average (or effective) distance of water transport process from the concrete around the aggregate into the

ASR gel, and $\eta(w_i)$ is an increasing function of w_i . Roughly, for two adjacent aggregate particles of diameters D_1 and D_2 , δ can be estimated as

$$\delta = \frac{l - D_1 - D_2}{2} \quad (15)$$

where l is the distance between the particle centers. The characteristic time, τ_i , must be an increasing function of w_i , because the imbibition of the layers of gel increases the diffusion time of the free water to reach the unimbibed gel. Therefore, it is reasonable to assume the function $\eta(w_i)$ as $\eta(w_i) = e^{\bar{\eta} w_i}$, in which $\bar{\eta}$ is a material constant.

By considering all these effects together, one has the following equation for water imbibition into the gel:

$$\dot{w}_i = \left(e^{-\frac{E_{aw}}{RT}} \xi_g - w_i \right) \frac{C_{wi}}{\delta^2} e^{-\bar{\eta} w_i} \quad (16)$$

The water imbibed into the gel is given by the following differential equation:

$$\dot{w}_i = \left[e^{-\frac{E_{aw}}{RT}} \frac{4\pi D^3}{3 \cdot 8} (1 - \zeta^3) \frac{m_g}{m_s} \rho_s \rho_k - w_i \right] \cdot \frac{C_{wi}}{\delta^2} e^{-\bar{\eta} w_i} \quad (17)$$

3 LATTICE DISCRETE PARTICLE MODEL

LDPM simulates concrete mesostructure by taking into account only the coarse aggregate pieces, typically with characteristic size greater than about 4 mm. The mesostructure is constructed through the following steps. 1) The coarse aggregate pieces, whose shapes are assumed to be spherical, are introduced into the concrete volume by a try-and-reject random procedure. 2) Zero-radius aggregate pieces (nodes) are randomly distributed over the external surfaces. 3) A three-dimensional domain tessellation, based on the Delaunay tetrahedralization of the generated aggregate centers, creates a system of cells interacting through triangular facets, which can be represented, in a two-dimensional setting, by straight line segments as shown in Figure 3. A vectorial constitutive law governing the behavior of the model is imposed at the centroid of the projection of each

single facet (contact point) onto a plane orthogonal to the straight line connecting the particle centers (edges of the tetrahedralization). The projections are used instead of the facets themselves to ensure that the shear interaction between adjacent particles does not depend on the shear orientation. The straight lines connecting the particle centers define the lattice system.

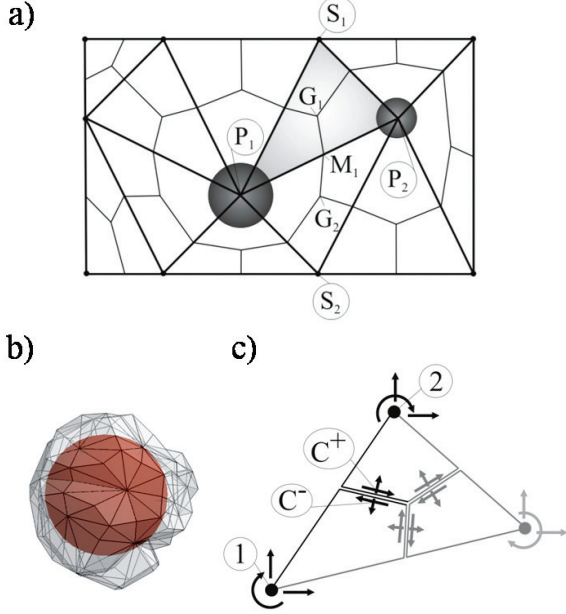


Figure 3: a) Mesostructure tessellation. b) Three-dimensional discrete particle. c) Definition of nodal degrees of freedom and contact facets in two-dimensions.

Rigid body kinematics describes the displacement field along the lattice struts and the displacement jump, $[\mathbf{u}_C]$, at the contact point. The strain vector is defined as the displacement jump at the contact point divided by the inter-particle distance, L . The components of the strain vector in a local system of reference, characterized by the unit vectors \mathbf{n} , \mathbf{l} , and \mathbf{m} , are the normal and shear strains:

$$\begin{aligned}\varepsilon_N &= \frac{\mathbf{n}^T[\mathbf{u}_C]}{L}; \varepsilon_L = \frac{\mathbf{l}^T[\mathbf{u}_C]}{L}; \\ \varepsilon_M &= \frac{\mathbf{m}^T[\mathbf{u}_C]}{L}\end{aligned}\quad (18)$$

The unit vector \mathbf{n} is orthogonal to the projected facet and the unit vectors \mathbf{l} and \mathbf{m} are mutually orthogonal and lie in the projected facet.

The elastic behavior is described by assuming that the normal and shear stresses are proportional to the corresponding strains:

$$\sigma_N = E_N \varepsilon_N; \sigma_M = E_T \varepsilon_M; \sigma_L = E_T \varepsilon_L \quad (19)$$

where $E_N = E_0$, $E_T = \alpha E_0$, $E_0 =$ effective normal modulus, and $\alpha =$ shear-normal coupling parameter. E_0 and α are assumed to be material properties. Detailed description of model behavior in the nonlinear range can be found in Ref. [6]. Current LDPM formulation has been implemented into MARS, a multi-purpose computational code for the explicit dynamic simulation of structural performance [15].

4 AMALGAMATION OF ASR MODEL WITHIN LDPM FRAMEWORK

The radius variation of one aggregate particle can be calculated from the volume variation in Equation 11 as

$$\Delta r = \sqrt[3]{\frac{3\Delta V}{4\pi} + \frac{D^3}{8}} - D/2 \quad (20)$$

The calculated aggregate radius variation is used to calculate the LDPM imposed ASR gel strain, ε_{N0} as

$$\varepsilon_{N0} = (\Delta r_1 + \Delta r_2 - \delta_c)/L \quad (21)$$

where Δr_1 and Δr_2 are the radii changes of two adjacent aggregate particles. This additional normal strain is imposed on the LDPM facet by adding it to the stress-dependent facet normal strain. In the elastic regime, one can write the normal stress as $\sigma_N = E_N(\varepsilon_N - \varepsilon_{N0})$. Note that the model formulated here approximately assumes that the facet shear deformations due to gel swelling are negligible, $\varepsilon_{M0} = \varepsilon_{L0} \approx 0$, although this might not be exactly true due to the irregularity of actual aggregate particles.

5 NUMERICAL SIMULATIONS

In this study, simulation of experimental results of Multon and Toutlemonde [16] was performed as described in the following sections. These accelerated experiments have

shown good representation to the actual long term phenomena as they could represent the expansion growth the same model used by Larive et al [17] to express dams ASR expansions. In the following sections, an automatic parameter identification technique based on the nonlinear least square method is used throughout all calibrations to identify different model parameters.

5.1 ASR model free parameters

The proposed model contains material parameters that need to be defined. Some parameters, such as activation energies E_{aw} and E_{ad} , reference ASR gel permeability to water a_{s0} , required and threshold alkali contents AC_{req} and AC_{th} , and silica content ρ_s , can be determined directly if specific experimental data such as diffusion tests and permeability tests and/or aggregate chemical analysis are available. Others, such as δ_c , C_{wi} , and $\bar{\eta}$ are very hard to measure and they need to be calibrated by inverse analysis of macroscopic experimental results. The remaining parameters are either well defined or easy to assume as water content w_s , current alkali content AC , T and T_0 . Throughout the simulations, some parameters were assumed as follows: ρ_s was assumed to be about 20% of the total aggregate mass so by weight it equals $0.2 \cdot 2200 \text{ kg/m}^3$ (silica unit weight) = 440 kg/m^3 . The presence of silica in aggregate varies based on the aggregate type and it can reach up to $50\% \pm 10\%$ as reported in [18]. The free water content, w_s , can be reasonably assumed using the relation given by [19] as $w_s = (w/c - (0.235 + 0.19) \cdot \alpha_c) \cdot c$, where w/c , α_c and c are the water cement ratio, reaction degree and cement content in kg/m^3 .

5.2 Calibration of LDPM concrete parameters

To match the concrete mechanical properties relevant to the analyzed experimental data, LDPM parameters were calibrated based on reported values of compressive strength, f'_c , Young's modulus, E and splitting tensile strength, f'_t . Ten numerical specimens with different meso-structures were always simu-

lated and their average response was considered. The generation of the different LDPM meso-structures was performed considering the grain size distribution of the specimens used in the experimental campaign as shown in Figure 4. The calibration of LDPM parameters gave the results shown in Table 1.

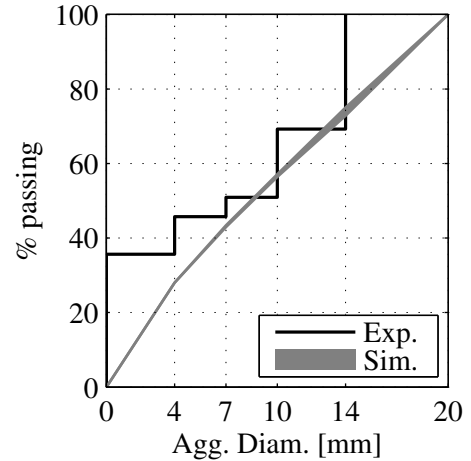


Figure 4: Grain Size distribution for simulated and experimental specimens

Table 1: Mechanical properties

Property	Actual	Simulated Average
f'_c (MPa)	38.4	38.41
f'_t (MPa)	3.2	3.19
E (MPa)	37300	37695

5.3 Creep and shrinkage consideration.

The experimental results show, for the control specimens, autogenous shrinkage of the order 0.25%. To account for the shrinkage, the CEB MC99 model was adopted for shrinkage as it divides the shrinkage into autogenous and drying parts. Figure 5 shows the calibration results of the model along with experimental data. Also for the loaded cases in the experimental campaign, the results show a considerable amount of creep. To account for creep deformation, the B3 model was adopted. Figure 6 shows the calibrated creep model as well as the experimental data. Both creep and shrinkage strains are added to the simulated strain re-

sults and compared with the experimental reported measured strains.

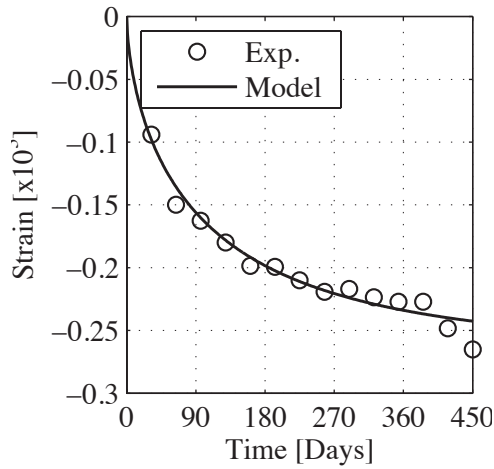


Figure 5: Calibration of Shrinkage Strain with CEB MC99 model.

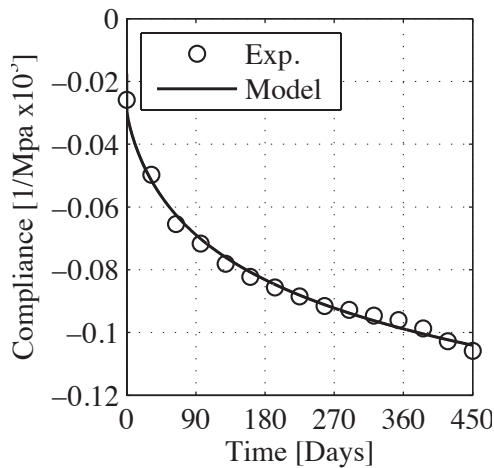


Figure 6: Calibration of Creep Strain with B3 model

5.4 Calibration of ASR model parameters with free expansion results.

Since the analyzed experiments of Multon and Toutlemonde [16] are relevant to an accelerated reaction (450 days compared to 5 to 50 years in dams), and with big fraction of reactive aggregate (all aggregates 4 mm in diameter and above were reactive giving 64.5% by weight) and high alkali content, δ_c tends to be zero as almost all pores surrounding the near aggregate surface were filled quickly in the early 28 days

of curing. The parameters providing the temperature dependence (E_{aw} and E_{ad}) were reasonably assumed on the basis of existing literature as in Ref. [?] and E_{aw} was also assumed to be equal to E_{ad} . Also as there was no data about the temperature values during the test it was assumed to be the room temperature of 23 °C. On the contrary, the other parameters (a_{s0} , δ_c , C_{wi} and $\bar{\eta}$) were calibrated using the automatic parameter identification procedure based on available volumetric measured strains. The average responses of volumetric strains for the ten simulated specimens after adding shrinkage strains, as well as the experimental data averages, are shown in Figure 7.

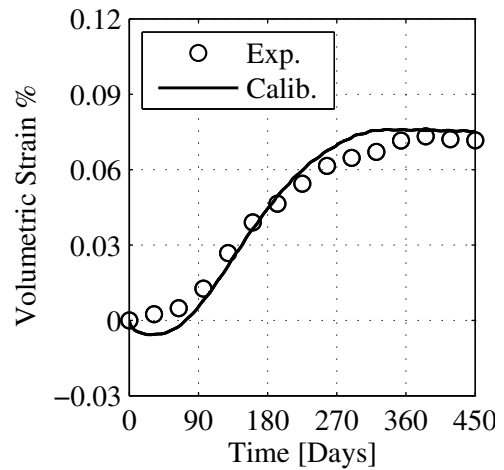


Figure 7: Free Expansion calibration based on Volumetric Strain

Figure 8: Free Expansion Axial and Radial Strains

Also the model could replicate the anisotropy found in the experimental results of free expansion by Multon and Toutlemonde [16], which is a unique feature of the model that can not be done without explicitly defining anisotropic properties for the model, while here only the different random geometry could simulate it. Figure 8 shows both axial and radial strains for the free expansion case for both experimental and simulated cases showing also the scatter of experimental data. The values of

the calibrated, as well as the assumed parameters, are listed in Table 2. In these experiments, there was no study for the temperature effects so, the activation energies have no effect on simulations.

Table 2: Used ASR Model Parameters

Parameter	Value	Type
w_s (kg/m ³)	56.662	Assumed
ρ_s (kg/m ³)	440	Assumed
ρ_k	1	Assumed
a_{s0} (m ² /s)	$9.7407 \cdot 10^{-9}$	Calibrated
E_{aw} (Joule/mole)	-	Assumed
E_{ad} (Joule/mole)	-	Assumed
δ_c (m)	0.0	Assumed
C_{wi} (m ² /s)	$3.4552 \cdot 10^{-13}$	Calibrated
$\bar{\eta}$ (kg ⁻¹)	36813	Calibrated

5.5 Simulation of axially loaded unrestrained specimens with 10MPa and 20MPa.

After parameter calibration, all the parameters were kept fixed and the simulations were carried out for the axially loaded unrestrained specimens. Two different axially loaded unrestrained specimens were considered: the first with 10 MPa and the second with 20 MPa. Ten generated specimens were used and their responses along with the experimental results for both axial and radial strains are shown in Figures 9 and 10, which show an excellent agreement between simulations and experimental data.

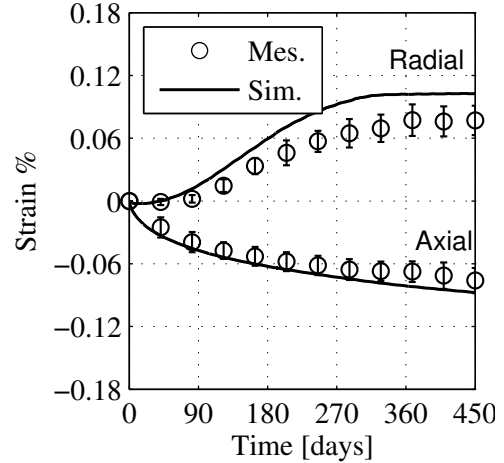


Figure 9: Unrestrained Expansion under 10 MPa Axial and Radial Strains

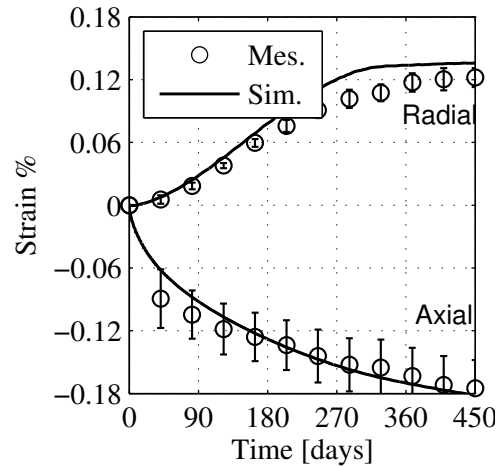


Figure 10: Unrestrained Expansion under 20 MPa Axial and Radial Strains

5.6 Simulated Crack patterns

One of the unique advantages of implementing this ASR model within the LDPM framework is the capability of reproducing the very scattered and heterogenous crack patterns that closely resemble crack patterns reported in experiments. This is illustrated in Figures 11 and 12. The cracks shown represent cracks with openings larger 0.015 mm. In Figure 11, it is clear that each simulated specimen has its own different crack patterns however all the three specimens responses showed reasonable visual agreement with typical experimental data in the literature [2].

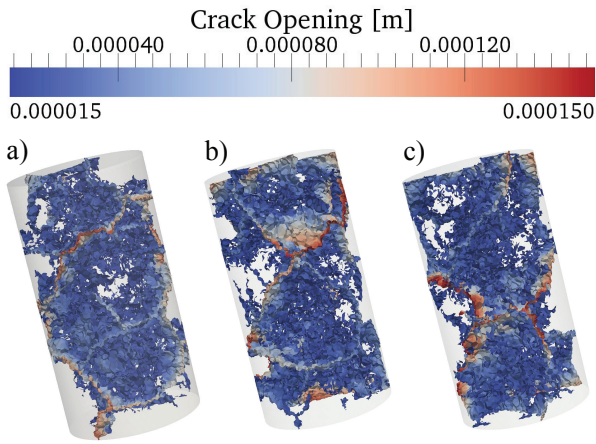


Figure 11: Crack distribution under free expansion for: a) Specimen n.1, b) Specimen n.3, c) Specimen n.9

Also by examining the surface cracks as well as internal cracks shown here, the very random character of cracking can be identified as well as the characteristic of having wider crack openings on the external surface can be shown clearly. This feature emphasizes the capability of the model to reproduce realistic crack propagation simulation.

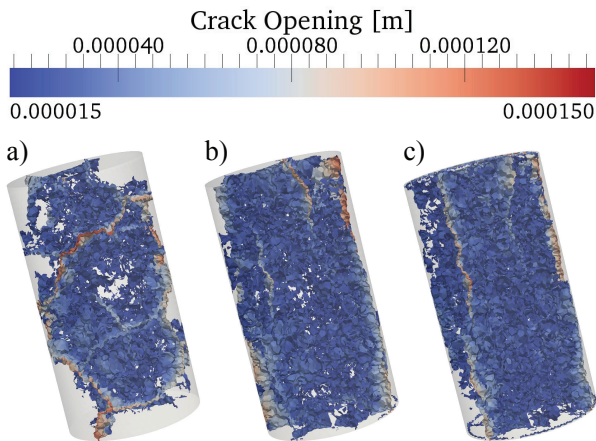


Figure 12: Crack distribution for Specimen n.1 under: a) Free Expansion, b) 10 MPa, c) 20 MPa

Moreover, the effect of axial loading on the size and distribution of cracks is shown in Figure 12 for specimen n. 1. It is clear that the cracks for the free expansion case are randomly distributed with no clear preferential direction, but on the contrary, cracks for both axially loaded cases show redirection in the radial

direction (cracks are aligned in vertical direction).

Since the gel expansion is constrained in the concrete microstructure, the gel volume increase produces a pressure, which in turn causes cracking in the concrete meso-structure. The presence of triaxial stress state reduces the ASR induced expansion in the less compressed direction leading to the so-called ASR anisotropic development which is commonly modeled using the concept of "Expansion transfer" [16, 20, 21]. In the current formulation, no gel redirection is postulated. The redirection of ASR imposed strain is interpreted as only redirection of crack distribution. While some authors in [16, 20, 21] refer to ASR induced expansion as a volumetric expansions to be calculated for the different states of stresses, here, the effect of ASR expansion is decomposed into its two components, gel volume increase due to water imbibition and crack volume generated. With this unique decoupling and considering the heterogeneity of the material by means of LDPM, deeper analysis of the effect of stress was possible, leading to postulating that the real effect of stress state is the reduction of cracking in the direction of higher compression and the increase of cracking in the other directions. This is also supported by the low likelihood for the solid gel [14] to migrate easily under stress effect through the concrete meso-structure. By observing both the responses shown in Figures 8, 9 and 10 as well as the crack distribution redirection shown in Figure 12, it can be seen clearly that the model could capture the "Expansion transfer" effect.

6 CONCLUSIONS

A model that simulate the ASR effect has been implemented within the framework of a mesoscale formulation, such as the Lattice Discrete Particle Model. This model has been used for the numerical simulations of experimental data reported by Multon and Toutlemonde [16]. Based on the observed results, the following conclusions can be drawn:

1. The model can accurately simulate free expansion experimental data and can reproduce realistic crack patterns.
2. Axial loading simulations show good agreement with experimental results, especially the crack patterns demonstrate the ability of the model to redirect cracking based on the stress state.
3. The expansion transfer concept can be modeled by decoupling the gel expansion from crack volume and by this, the stress state will only affect the crack distribution and there is no need to assume that the ASR gel migrates under stress state changes.

ACKNOWLEDGEMENTS

The authors gratefully acknowledge financial support under DHS grant 2010-ST-108-000016 entitled High Strain Rate Behavior of Dam Concrete: Experiments and Multiscale Modeling.

REFERENCES

- [1] G. Giaccio, R. Zerbino, J.M. Ponce, and O. R. Batic, 2008. Mechanical behavior of concretes damaged by alkali-silica reaction. *Cement and Concrete Research*, **38**:993–1004.
- [2] V. Saouma and Y. Xi, 2004. Literature Review of Alkali Aggregate Reactions in Concrete Dams. Report cu/sa-xi-2004/001, *Department of Civil, Environmental, & Architectural Engineering University of Colorado*.
- [3] Z.P. Bažant and A. Steffens, 2000. Mathematical model for kinetics of alkali-silica reaction in concrete. *Cement and Concrete Research*, **30**:419–428.
- [4] G. Cusatis, G. Di Luzio, and L. Cedolin, 2011. Meso-Scale Simulation of Concrete: Blast and Penetration Effects and AAR Degradation. *Applied Mechanics and Materials*, **82**:75–80.
- [5] G. Di Luzio, M. Alnaggar, and G. Cusatis, 2012. Lattice discrete particle modeling of alkali-silica-reaction effects to concrete structures. In P. Rossi and J.L. Tailhan, editors, *Numerical Modeling - Strategies for Sustainable Concrete Structures-SSCS 2012*. Aix en Provence, France.
- [6] G. Cusatis, D. Pelessone, and A. Mencarelli, 2011. Lattice Discrete Particle Model (LDPM) for Concrete failure Behavior of Concrete. I: Theory. *Cement and Concrete Composites*, **33**(9):881–890.
- [7] G. Cusatis, A. Mencarelli, D. Pelessone, and J.T. Baylot, 2011. Lattice Discrete Particle Model (LDPM) for Failure Behavior of Concrete. II: Calibration and Validation. *Cement and Concrete Composites*, **33**(9):891–905.
- [8] R. Dron and F. Brivot, 1992. Thermodynamic and kinetic approach to the alkali-silica reaction: Part 1. *Cement and Concrete Research*, **22**(5):941–948.
- [9] R. Dron and F. Brivot, 1993. Thermodynamic and kinetic approach to the alkali-silica reaction: Part 2. *Cement and Concrete Research*, **23**(1):93–103.
- [10] Z.P. Bažant and L.J. Najjar, 1972. Non-linear water diffusion in nonsaturated concrete. *Material and Structures*, **5**(25):3–20.
- [11] M. Jooss and H.W. Reinhardt, 2002. Permeability and diffusivity of concrete as function of temperature. *Cement and Concrete Research*, **32**(9):1497–1504.
- [12] G. Di Luzio and G. Cusatis, 2009. Hygrothermo-chemical modeling of high performance concrete. I: Theory. *Cement and Concrete Composites*, **31**(5):301–308.
- [13] G. Di Luzio and G. Cusatis, 2009. Hygrothermo-chemical modeling of high performance concrete. II: Numerical implementation, calibration, and validation. *Cement*

- and Concrete Composites*, **31**(5):309–324.
- [14] T.C. Powers and H.H. Steinour, 1955. An Interpretation of Some Published Researches on the Alkali-Aggregate Reaction'. *Journal of American Concrete Institute (Proc.)*, **55**:497–516 and 785–812.
- [15] D. Pelessone, 2009. *MARS: Modeling and Analysis of the Response of Structures - User's Manual*. ES3, Beach (CA), USA.
- [16] S. Multon and F. Toutlemonde, 2006. Effect of applied stresses on alkali-silica reaction-induced expansions. *Cement and Concrete Research*, **36**:912–920.
- [17] F. Ulm, O. Coussy, L. Kefei, and C. Larive, 2000. Thermo-Chemo-Mechanics Of ASR Expansion In Concrete Structures. *Journal of Engineering Mechanics*, **126**(3):233–242.
- [18] N. Castro, B. E. Sorensen, and M. A.T.M. Broekmans, 2011. Assessment of individual ASR-Aggregate particles by XRD. *Proceedings of the 10th International Congress for Applied Mineralogy (ICAM)*, pages 95–102.
- [19] O. Jensen and P. Hansen, 2001. Water-entrained cement-based materials I. Principles and theoretical background. *Cement and Concrete Research*, **31**:647–654.
- [20] C. Larive, A. Laplaud, and M. Joly, 1996. Behavior of AAR-affected concrete: experimental data. *Proc. 10th Int. Conf. AAR, Melbourne, Australia*, pages 670–677.
- [21] S. Multon, G. Leclainche, E. Bourdarot, and F. Toutlemonde, 2004. Alkali-silica reaction in specimens under multi-axial mechanical stresses. *Proc. 4th Int. Conf. CONSEC'04, Seoul, Korea*, pages 2004–2011.